Detroux, T., Renson, L., Masset, L., & Kerschen, G. (2016). The harmonic balance method for bifurcation analysis of nonlinear mechanical systems. In G. Kerschen (Ed.), Dynamic Behavior of Materials: Proceedings of the 33rd IMAC, A Conference and Exposition on Structural Dynamics, 2015. (Vol. 1, pp. 65-82). (Conference Proceedings of the Society for Experimental Mechanics Series). Springer New York LLC. DOI: 10.1007/978-3-319-15221-9_5

The Harmonic Balance Method for Bifurcation Analysis of Nonlinear Mechanical Systems

T. Detroux, L. Renson, L. Masset, G. Kerschen

Space Structures and Systems Laboratory (S3L), Structural Dynamics Research Group

Department of Aerospace and Mechanical Engineering, University of Liège, Belgium

Abstract

Because nowadays structural engineers are willing to use or at least understand nonlinearities instead of simply avoiding them, there is a need for numerical tools performing analysis of nonlinear large-scale structures. Among these techniques, the harmonic balance (HB) method is certainly one of the most commonly used to study finite element models with reasonably complex nonlinearities. However, in its classical formulation the HB method is limited to the approximation of periodic solutions. For this reason, the present paper proposes to extend the method to the detection and tracking of codimension-1 bifurcations in the system parameters space. As an application, the frequency response of a spacecraft is studied, together with two nonlinear phenomena, namely quasiperiodic oscillations and detached resonance curves. This example illustrates how bifurcation tracking using the HB method can be employed as a promising design tool for detecting and eliminating such undesired behaviors.

Keywords: continuation of periodic solutions, bifurcation tracking, harmonic balance method, quasiperiodic oscillations, detached resonance curves.

1 INTRODUCTION

As engineering structures are designed to be lighter and operate in more severe conditions, nonlinear phenomena such as amplitude jumps, modal interactions, limit cycle oscillations and quasiperiodic (QP) oscillations are expected to occur[1]. These are phenomena that can be frequently encountered in normal operation regime, in space[2, 3] and aeroelastic[4] applications, or during GVT campaigns[5, 6]. Classical excitation signals as swept-sine and harmonic tests can already reveal nonlinear behaviors. For most of these nonlinear structures, bifurcations play a key role in the response dynamics; for example, fold bifurcations indicate a stability change for the periodic solutions, while QP oscillations are encountered in the vicinity of Neimark-Sacker (NS) bifurcations. In that regard, it seems relevant to include analysis of bifurcations while performing a parametric study of the structure.

Different algorithms and numerical methods can be found in the literature for the computation of periodic solutions and their bifurcations. Most of them build on a continuation procedure[7], as a way to study the evolution of the solutions with respect to a certain parameter, e.g., the frequency of an external excitation or a system parameter. Time domain methods, which deal with the resolution of a boundary value problem (BVP), usually prove accurate for low-dimensional structures. When applied to larger systems however, their computational burden become substantial. For example, the shooting technique[8] requires numerous time integrations that can drastically slow down the speed of the algorithm. Methods based on the orthogonal collocation, which uses a discretization of the BVP, are widely utilized in software for bifurcation detection and tracking like AUTO[9], COLSYS[10], CONTENT[11], MATCONT[12] or, more recently, COCO[13]. In spite of its high accuracy and ability to address problems with singularities, orthogonal collocation is rarely employed to study large systems, which can be explained by the considerable memory space this method requires for the discretization of the problem.

Among all methods in the frequency domain, the harmonic balance (HB) method, also known as the Fourier–Galerkin method, is certainly the most widely used. It approximates the periodic signals with their Fourier coefficients, which become the new unknowns of the problem. First implemented for analyzing linear systems, the HB method was then successfully adapted to nonlinear problems, in electrical[14] and mechanical engineering[15, 16] for example. The main advantage of the HB method is that it involves algebraic equations with less unknowns than the methods in the time domain, for problems for which low orders of approximation are sufficient to obtain an accurate solution; this is usually the case if the regime of the system is not strongly nonlinear. For this reason, the HB method has received increased attention for the last couple of years, which has led to numerous applications and adaptations of the method[17–19] and to the development of a continuation package MANLAB[20, 21]. The readers can also refer to [22] for a comparison between the HB method and orthogonal collocation in terms of convergence. Nevertheless, in spite of its performance and accuracy, to the authors' knowledge the HB method has never been extended to track bifurcations. In a previous work[23], the authors laid down the foundations for this extension, through the application to a system with 2 degrees of freedom (DOFs). The purpose of this work is to provide implementation details to track bifurcations of larger structures, and to illustrate how the tracking procedure can reveal and explain unexpected nonlinear phenomena.

The first part of this paper is devoted to the HB theory and its formulation in the framework of a continuation algorithm. Then Hill's method is introduced to assess the stability of periodic solutions, and to detect their bifurcations. The bifurcation tracking procedure is finally presented with its adaptations for branch point, fold and NS bifurcations. As an application, the analysis of the nonlinear dynamics of an industrial spacecraft is proposed. Starting from swept-sine and harmonic responses, nonlinear phenomena are highlighted and then studied through bifurcation detection and tracking.

2 HARMONIC BALANCE METHOD

This section first performs a brief review of the theory of the HB method. The method will be applied to general non-autonomous nonlinear dynamical systems with n DOFs whose equations of motion are

$$\mathbf{M}\ddot{\mathbf{x}} + \mathbf{C}\dot{\mathbf{x}} + \mathbf{K}\mathbf{x} = \mathbf{f}_{ext}(\omega, t) - \mathbf{f}_{nl}(\mathbf{x}, \dot{\mathbf{x}}) = \mathbf{f}(\mathbf{x}, \dot{\mathbf{x}}, \omega, t) \tag{1}$$

where $\mathbf{M}$,$\mathbf{C}$ and $\mathbf{K}$ are the mass, damping and stiffness matrices respectively, $\mathbf{x}$ represents the displacements, the dots refer to the derivatives with respect to time t, $\mathbf{f}_{nl}$ represents the nonlinear forces and $\mathbf{f}_{ext}$ stands for the periodic external forces (harmonic excitation, for example) with frequency ω. The term $\mathbf{f}$ gathers both the external and nonlinear forces.

As recalled in the introduction, the periodic solutions $\mathbf{x}(t)$ and $\mathbf{f}(t)$ of equation (1) are approximated by Fourier series truncated to the N_H-th harmonic:

$$\begin{aligned} \mathbf{x}(t) &= \mathbf{c}_0^x + \textstyle\sum_{k=1}^{N_H} \left(\mathbf{s}_k^x \sin\left(\frac{k\omega t}{\nu}\right) + \mathbf{c}_k^x \cos\left(\frac{k\omega t}{\nu}\right)\right) \\ \mathbf{f}(t) &= \mathbf{c}_0^f + \textstyle\sum_{k=1}^{N_H} \left(\mathbf{s}_k^f \sin\left(\frac{k\omega t}{\nu}\right) + \mathbf{c}_k^f \cos\left(\frac{k\omega t}{\nu}\right)\right) \end{aligned} \tag{2}$$

where $\mathbf{s}_k$ and $\mathbf{c}_k$ represent the vectors of the Fourier coefficients related to the sine and cosine terms, respectively. Here it is interesting to note that the Fourier coefficients of $\mathbf{f}(t)$, $\mathbf{c}_k^f$ and $\mathbf{s}_k^f$, depend on the Fourier coefficients of the displacements $\mathbf{x}(t)$, $\mathbf{c}_k^x$ and $\mathbf{s}_k^x$. The integer parameter ν is introduced to account for some possible subharmonics of the external excitation frequency ω.

Substituting expressions (2) in equations (1) and balancing the harmonic terms with a Galerkin projection yields the following nonlinear equations in the frequency domain

$$\mathbf{h}(\mathbf{z}, \omega) \equiv \mathbf{A}(\omega)\mathbf{z} - \mathbf{b}(\mathbf{z}, \omega) = \mathbf{0} \tag{3}$$

where $\mathbf{A}$ is the $(2N_H + 1)\, n \times (2N_H + 1)\, n$ matrix describing the linear dynamics of the system, $\mathbf{z}$ is the vector containing all the Fourier coefficients of the displacements $\mathbf{x}(t)$, and $\mathbf{b}$ represents the vector of the Fourier coefficients of the external and nonlinear forces $\mathbf{f}(t)$. They have the following expressions:

$$\mathbf{A} = \begin{bmatrix} \mathbf{K} & & & & \\ & \mathbf{K} - \left(\frac{\omega}{\nu}\right)^2 \mathbf{M} & -\frac{\omega}{\nu}\mathbf{C} & & \\ & \frac{\omega}{\nu}\mathbf{C} & \mathbf{K} - \left(\frac{\omega}{\nu}\right)^2 \mathbf{M} & & \\ & & & \ddots & \\ & & & \mathbf{K} - \left(N_H \frac{\omega}{\nu}\right)^2 \mathbf{M} & -N_H \frac{\omega}{\nu}\mathbf{C} \\ & & & N_H \frac{\omega}{\nu}\mathbf{C} & \mathbf{K} - \left(N_H \frac{\omega}{\nu}\right)^2 \mathbf{M} \end{bmatrix}, \quad \mathbf{z} = \begin{bmatrix} \mathbf{c}_0^x \\ \mathbf{s}_1^x \\ \mathbf{c}_1^x \\ \vdots \\ \mathbf{s}_{N_H}^x \\ \mathbf{c}_{N_H}^x \end{bmatrix}, \quad \mathbf{b} = \begin{bmatrix} \mathbf{c}_0^f \\ \mathbf{s}_1^f \\ \mathbf{c}_1^f \\ \vdots \\ \mathbf{s}_{N_H}^f \\ \mathbf{c}_{N_H}^f \end{bmatrix} \tag{4}$$

In the time domain, expression (1) contains n equations while, in the frequency domain, expression (3) have $(2N_H + 1)\, n$ unknowns gathered in $\mathbf{z}$. Expression (3) can be seen as the equations of amplitude of (1): if $\mathbf{z}^*$ is a root of (3), then the time signals $\mathbf{x}^*$ constructed from $\mathbf{z}^*$ with (2) are solutions of the equations of motion (1) and are periodic.

2.1 Analytical expression of the nonlinear terms and of the jacobian matrix of the system

Since $\mathbf{b}$ depends on $\mathbf{z}$, equation (3) is nonlinear and has to be solved iteratively (e.g., with a Newton-Raphson procedure). At each iteration, an evaluation of $\mathbf{b}$ and of $\partial\mathbf{h}/\partial\mathbf{z}$ has to be provided. If the nonlinearity is weak, in some cases $\mathbf{f}$ can be accurately approximated with a few number of harmonics N_H, and analytical relations between the Fourier coefficients of the forces $\mathbf{b}$ and of the displacements $\mathbf{z}$ can be developed together with the expression of the jacobian of the system[24–26]. When such developments are too intricate, most of the studies in the literature propose to evaluate $\mathbf{b}$ through successive transformations from frequency to time domains. For example, the alternating frequency/time-domain (AFT) technique[27] takes advantage of the fast Fourier transform to compute $\mathbf{b}$:

$$\mathbf{z} \xrightarrow{\text{FFT}^{-1}} \mathbf{x}(t) \rightarrow \mathbf{f}\left(\mathbf{x}, \dot{\mathbf{x}}, \omega, t\right) \xrightarrow{\text{FFT}} \mathbf{b}(\mathbf{z}, \omega) \tag{5}$$

The jacobian matrix of the system can then be computed through finite differences, which is cumbersome in terms of CPU time, or through linearization of the equations[15].

An efficient alternative consists in rewriting the inverse Fourier transform as a linear operator $\mathbf{\Gamma}\left(\omega\right)$[28–31]. First, denoting N as the number of time samples of a discretized period of oscillation, one defines vectors $\tilde{\mathbf{x}}$ and $\tilde{\mathbf{f}}$ containing the concatenated nN time samples of the displacements and the forces, respectively, for all the DOFs:

$$\tilde{\mathbf{x}} = \begin{bmatrix} x_1\left(t_1\right) \\ \vdots \\ x_1\left(t_N\right) \\ \vdots \\ x_n\left(t_1\right) \\ \vdots \\ x_n\left(t_N\right) \end{bmatrix}, \qquad \tilde{\mathbf{f}} = \begin{bmatrix} f_1\left(t_1\right) \\ \vdots \\ f_1\left(t_N\right) \\ \vdots \\ f_n\left(t_1\right) \\ \vdots \\ f_n\left(t_N\right) \end{bmatrix} \tag{6}$$

The inverse Fourier transform can then be written as a linear operation:

$$\tilde{\mathbf{x}} = \mathbf{\Gamma}\left(\omega\right) \mathbf{z} \tag{7}$$

with the $(nN \times (2N_H + 1)\, n)$ sparse operator

$$\boldsymbol{\Gamma}(\omega) =$$

$$\left[\begin{array}{c} \\ \mathbb{I}_n \otimes \left[\begin{array}{c} 1 \\ 1 \\ \vdots \\ 1 \end{array} \right] \\ \\ \end{array} \quad \mathbb{I}_n \otimes \left[\begin{array}{c} \sin(\omega t_1) \\ \sin(\omega t_2) \\ \vdots \\ \sin(\omega t_N) \end{array} \right] \quad \mathbb{I}_n \otimes \left[\begin{array}{c} \cos(\omega t_1) \\ \cos(\omega t_2) \\ \vdots \\ \cos(\omega t_N) \end{array} \right] \quad \cdots \quad \mathbb{I}_n \otimes \left[\begin{array}{c} \sin(N_H \omega t_1) \\ \sin(N_H \omega t_2) \\ \vdots \\ \sin(N_H \omega t_N) \end{array} \right] \quad \mathbb{I}_n \otimes \left[\begin{array}{c} \cos(N_H \omega t_1) \\ \cos(N_H \omega t_2) \\ \vdots \\ \cos(N_H \omega t_N) \end{array} \right] \right] \tag{8}$$

where $\otimes$ and $\mathbb{I}$ stand for the Kronecker tensor product and the identity matrix, respectively. The direct Fourier transformation is written

$$\mathbf{z} = \left(\boldsymbol{\Gamma}(\omega)\right)^{+} \tilde{\mathbf{x}} \tag{9}$$

where $^{+}$ stands for the Moore-Penrose pseudoinverse:

$$\boldsymbol{\Gamma}^{+} = \boldsymbol{\Gamma}^{T} \left(\boldsymbol{\Gamma}\boldsymbol{\Gamma}^{T}\right)^{-1} \tag{10}$$

According to these notations, the Fourier coefficients of the external and nonlinear forces are simply obtained by transforming the signals in the time domain back to the frequency domain:

$$\mathbf{b}(\mathbf{z}, \omega) = \left(\boldsymbol{\Gamma}(\omega)\right)^{+} \tilde{\mathbf{f}} \tag{11}$$

The jacobian matrix of expression (3) with respect to the Fourier coefficients $\mathbf{z}$ can be computed as

$$\mathbf{J}_z = \frac{\partial \mathbf{h}}{\partial \mathbf{z}} = \mathbf{A} - \frac{\partial \mathbf{b}}{\partial \mathbf{z}} \tag{12}$$

In order to compute the derivative of $\mathbf{b}$ with respect to the Fourier coefficients of the displacements, $\mathbf{z}$, one can use the following chain rule:

$$\frac{\partial \mathbf{b}}{\partial \mathbf{z}} = \frac{\partial \mathbf{b}}{\partial \tilde{\mathbf{f}}} \frac{\partial \tilde{\mathbf{f}}}{\partial \tilde{\mathbf{x}}} \frac{\partial \tilde{\mathbf{x}}}{\partial \mathbf{z}} \tag{13}$$

which is rewritten with the transformation matrices

$$\frac{\partial \mathbf{b}}{\partial \mathbf{z}} = \boldsymbol{\Gamma}^{+} \frac{\partial \tilde{\mathbf{f}}}{\partial \tilde{\mathbf{x}}} \boldsymbol{\Gamma} \tag{14}$$

In general, the derivatives of the forces with respect to the displacements in the time domain can be expressed analytically, which makes the computation of the jacobian matrix of (3) faster than with the finite differences.

2.2 Continuation procedure

It is usually of interest to solve (3) for a range of parameter values ω, rather than for a single value of the parameter. One could for example be interested in the behavior of a structure in the neighborhood of a resonance peak. A continuation scheme, coupled to the highlighted HB method, has therefore to be implemented.

Solving (3) for different fixed values of ω, as done with a sequential continuation procedure, fails at turning point. To overcome this issue, for this work a procedure based on tangent predictions and Moore-Penrose corrections has been selected, as proposed in the software MATCONT[12].

Denoting $\mathbf{J}_\omega$ as the jacobian of $\mathbf{h}$ with respect to the parameter ω, the search for a tangent vector $\mathbf{t}^{(i)}$ at an iteration point $\left(\mathbf{z}^{(i)}, \omega^{(i)}\right)$ along the branch reads

$$\begin{bmatrix} \mathbf{J}_z & \mathbf{J}_\omega \\ \mathbf{t}_{(i-1)}^T & \end{bmatrix} \mathbf{t}_{(i)} = \begin{bmatrix} \mathbf{0} \\ 1 \end{bmatrix} \tag{15}$$

The last equation in the system (15), imposing a scalar product of 1 between the new tangent and the previous one prevents the continuation procedure from turning back. For the first iteration of the procedure, this last row can be replaced by a condition imposing the sum of the components of the tangent to be equal to 1.

The correction stage is based on Newton's method. Introducing new optimization variables $\mathbf{v}_{(i,j)}$ initialized as $\mathbf{v}_{(i,1)} = \mathbf{t}_{(i)}$, and $\mathbf{y}_{(i,j)} = \left[\mathbf{z}_{(i,j)}\ \omega_{(i,j)}\right]^T$, the different Newton's iterations i are constructed as following:

$$\begin{aligned} \mathbf{y}_{(i,j+1)} &= \mathbf{y}_{(i,j)} - \mathbf{G}_y^{-1}\left(\mathbf{y}_{(i,j)}, \mathbf{v}_{(i,j)}\right) \mathbf{G}\left(\mathbf{y}_{(i,j)}, \mathbf{v}_{(i,j)}\right) \\ \mathbf{v}_{(i,j+1)} &= \mathbf{v}_{(i,j)} - \mathbf{G}_y^{-1}\left(\mathbf{y}_{(i,j)}, \mathbf{v}_{(i,j)}\right) \mathbf{R}\left(\mathbf{y}_{(i,j)}, \mathbf{v}_{(i,j)}\right) \end{aligned} \tag{16}$$

with

$$\mathbf{G}\left(\mathbf{y}, \mathbf{v}\right) = \begin{bmatrix} \mathbf{h}\left(\mathbf{y}\right) \\ \mathbf{0} \end{bmatrix}, \qquad \mathbf{G}_y\left(\mathbf{y}, \mathbf{v}\right) = \begin{bmatrix} \mathbf{J}_z\left(\mathbf{y}\right) & \mathbf{J}_\omega\left(\mathbf{y}\right) \\ \mathbf{v}^T & \end{bmatrix}, \qquad \mathbf{R}\left(\mathbf{y}, \mathbf{v}\right) = \begin{bmatrix} \begin{bmatrix} \mathbf{J}_z\left(\mathbf{y}\right) & \mathbf{J}_\omega\left(\mathbf{y}\right) \end{bmatrix} \mathbf{v} \\ \mathbf{0} \end{bmatrix} \tag{17}$$

For a more detailed presentation of the continuation procedure, the reader can refer to [12].

2.3 Stability analysis

The continuation procedure developed above does not indicate if a periodic solution is stable or not; therefore, a stability analysis has to be performed along the branch. In the case of time domain methods, such as the shooting technique, one usually obtains the monodromy matrix as a by-product of the procedure[8], which then provides the Floquet multipliers to study the stability of the solutions. On the other hand, in the case of frequency domain techniques such as the HB method, one preferably uses Hill's method by solving a quadratic eigenvalue problem whose components are obtained as by-products of the method. The quadratic eigenvalue problem proposed by von Groll *et al.*[16] for finding the Hill's coefficients as solutions of

$$\boldsymbol{\Delta}_2 \boldsymbol{\lambda}^2 + \boldsymbol{\Delta}_1 \boldsymbol{\lambda} + \mathbf{J}_z = \mathbf{0} \tag{18}$$

with

$$\boldsymbol{\Delta}_1 = \begin{bmatrix} \mathbf{C} & & & & & \\ & \mathbf{C} & -2\frac{\omega}{\nu}\mathbf{M} & & & \\ & 2\frac{\omega}{\nu}\mathbf{M} & \mathbf{C} & & & \\ & & & \ddots & & \\ & & & & \mathbf{C} & -2N_H\frac{\omega}{\nu}\mathbf{M} \\ & & & & 2N_H\frac{\omega}{\nu}\mathbf{M} & \mathbf{C} \end{bmatrix}, \qquad \boldsymbol{\Delta}_2 = \mathbb{I}_{(2N_H+1)} \otimes \mathbf{M} \tag{19}$$

can be rewritten as a linear eigenvalue problem of double size

$$\mathbf{B}_1 - \begin{bmatrix} \boldsymbol{\lambda} & \\ & \boldsymbol{\gamma} \end{bmatrix} \mathbf{B}_2 = \mathbf{0} \tag{20}$$

with

$$\mathbf{B}_1 = \begin{bmatrix} \boldsymbol{\Delta}_1 & \mathbf{J}_z \\ -\mathbb{I} & \mathbf{0} \end{bmatrix}, \qquad \mathbf{B}_2 = -\begin{bmatrix} \boldsymbol{\Delta}_2 & \mathbf{0} \\ \mathbf{0} & \mathbb{I} \end{bmatrix} \tag{21}$$

The eigenvalues $\boldsymbol{\lambda}$ can thus be found among the eigenvalues of the $(2N_H+1)\,2n \times (2N_H+1)\,2n$ matrix

$$\mathbf{B} = \mathbf{B}_2^{-1}\mathbf{B}_1 \tag{22}$$

However, only $2n$ eigenvalues $\tilde{\boldsymbol{\lambda}}$ among the set $\boldsymbol{\lambda}$ approximate the Floquet exponents of the solution[32]. The other eigenvalues are only spurious and do not have any physical meaning; their number also increases with the number of harmonics N_H. As way to extract the approximations of the Floquet exponents $\tilde{\boldsymbol{\lambda}}$ from the set $\boldsymbol{\lambda}$, Moore[33] showed that one should always choose the $2n$ eigenvalues with the smallest imaginary part in modulus. The term *Floquet exponents* will be used throughout this paper for the eigenvalues $\tilde{\boldsymbol{\lambda}}$; it should however be kept in mind that these exponents are computed with Hill's method. A diagonal matrix $\tilde{\mathbf{B}}$ containing the components of $\tilde{\boldsymbol{\lambda}}$ is then constructed:

$$\tilde{\mathbf{B}} = \begin{bmatrix} \tilde{\lambda}_1 & & & \\ & \tilde{\lambda}_2 & & \\ & & \ddots & \\ & & & \tilde{\lambda}_{2n} \end{bmatrix} \tag{23}$$

As will be explained in sections 2.4 and 2.5, this matrix $\tilde{\mathbf{B}}$ plays a key role in the detection and tracking of bifurcations.

2.4 Detection of bifurcations

In this work the detection and tracking of fold (F), Neimark-Sacker (NS) and branch point (BP) bifurcations is sought. The procedure proposed in this paper builds on the evaluation of *test functions* ϕ at each iteration along a continuation branch[12]; the roots of these test functions then indicate the presence of bifurcations.

According to their algebraic definitions, as explained by Seydel[34], a fold bifurcation is characterized by a rank deficiency of 1 for the jacobian matrix $\mathbf{J}_z$, and a BP bifurcation by a rank deficiency of 2. A necessary condition for fold and BP bifurcations is thus

$$|\mathbf{J}_z| = 0 \tag{24}$$

In order to distinguish between fold and BP bifurcations, Govaerts *et al*.[35] proposes the following test functions:

$$\begin{aligned} \phi_{BP} &= \begin{vmatrix} \mathbf{J}_z & \mathbf{J}_\omega \\ \mathbf{t}^T & \end{vmatrix} \\ \phi_{F,1} &= |\mathbf{J}_z| \end{aligned} \tag{25}$$

Fold bifurcations are found at roots of $\phi_{F,1}$, provided that ϕ_{BP} is different from 0.

One could also follow another approach, based on Floquet theory. A fold bifurcation is detected when a Floquet exponent crosses the imaginary axis along the real axis. As a consequence, the matrix of Floquet exponents $\tilde{\mathbf{B}}$ is singular at a fold bifurcation. One thus has an alternative test function $\phi_{F,2}$ written as

$$\phi_{F,2} = \left|\tilde{\mathbf{B}}\right| \tag{26}$$

The third type of bifurcation studied in this paper, the NS bifurcation, is detected when a pair of Floquet exponents crosses the imaginary axis as a pair of complex conjugates. Using the theory of the bialternate product[36] $\mathbf{P}_\odot$ of a $m \times m$ matrix $\mathbf{P}$

$$\mathbf{P}_\odot = \mathbf{P} \odot \mathbb{I}_m \tag{27}$$

which has the property to be singular when $\mathbf{P}$ has a pair of complex conjugates crossing the imaginary axis, one writes the test function for NS bifurcations as

$$\phi_{NS} = \left|\tilde{\mathbf{B}}_\odot\right| \tag{28}$$

Nevertheless, for large systems the values of determinants usually explode and their use leads to scaling problems. To overcome this issue, previous studies[37−39] proposed the so-called *bordering technique*. The idea behind this technique is to replace the evaluation of the determinant of a matrix $\mathbf{G}$ by the evaluation of a scalar function, herein denoted g, which vanishes as regular zero for the same system state and parameters as the determinant. Instead of

$$|\mathbf{G}| = 0 \tag{29}$$

it is more robust to write

$$g = 0 \tag{30}$$

where g is obtained by solving

$$\begin{bmatrix} \mathbf{G} & \mathbf{p} \\ \mathbf{q}^* & 0 \end{bmatrix} \begin{bmatrix} \mathbf{w} \\ g \end{bmatrix} = \begin{bmatrix} \mathbf{0} \\ 1 \end{bmatrix} \tag{31}$$

In this system, * denotes a conjugate transpose, and vectors $\mathbf{p}$ and $\mathbf{q}$ are chosen to ensure the nonsingularity of the matrix. When $\mathbf{G}$ is close to be singular, one preferably takes $\mathbf{q}$ and $\mathbf{p}$ close to the nullvectors of $\mathbf{G}$ and $\mathbf{G}^*$, respectively.

The test functions for BP, fold and NS bifurcations based on the bordering technique can finally be written as

$$\begin{array}{ll} \text{BP bifurcations:} & \phi_{BP} = g_{BP} \quad \text{with} \quad \mathbf{G}_{BP} = \begin{bmatrix} \mathbf{J}_z & \mathbf{J}_\omega \\ \mathbf{t}^T & \end{bmatrix} \\ \text{Fold bifurcations:} & \begin{cases} \phi_{F,1} = g_{F,1} \quad \text{with} \quad \mathbf{G}_{F,1} = \mathbf{J}_z \\ \text{or} \\ \phi_{F,2} = g_{F,2} \quad \text{with} \quad \mathbf{G}_{F,2} = \tilde{\mathbf{B}} \end{cases} \\ \text{NS bifurcations:} & \phi_{NS} = g_{NS} \quad \text{with} \quad \mathbf{G}_{NS} = \tilde{\mathbf{B}}_\odot \end{array} \tag{32}$$

It should be noted that it is also convenient to use another test function for fold detection, namely

$$\phi_{F,3} = \mathbf{t}_{i_\omega} \tag{33}$$

which describes the fact that a fold bifurcation is detected when the component i_ω of the tangent prediction related to the active parameter ω changes sign[35]. This function does not require the resolution of a bordered system and therefore reduces the computational burden.

2.5 Tracking of bifurcations

In order to continue codimension-1 bifurcations with respect to two parameters of the system, such as the frequency and amplitude of the forcing applied on the system, one has to append one equation to (3). Using the bordering technique, one obtains the following extended system:

$$\begin{cases} \mathbf{h} \equiv \mathbf{A}\mathbf{z} - \mathbf{b} = 0 \\ g = 0 \end{cases} \tag{34}$$

where $g = g_{BP}$, g_F and g_{NS} are the solutions of bordered systems for BP, fold and NS bifurcations, respectively, with

$$\begin{array}{ll} \text{BP bifurcations:} & \mathbf{G}_{BP} = \mathbf{J}_z \\ \text{Fold bifurcations:} & \begin{cases} \mathbf{G}_{F,1} = \mathbf{J}_z \\ \text{or} \\ \mathbf{G}_{F,2} = \tilde{\mathbf{B}} \end{cases} \\ \text{NS bifurcations:} & \mathbf{G}_{NS} = \tilde{\mathbf{B}}_\odot \end{array} \tag{35}$$

One notices that the same additional equation, that is the fact that the determinant of $\mathbf{J}_z$ is 0, can be used either for tracking fold or BP bifurcations. Again, for fold bifurcations, one can follow either the algebraic approach using $\mathbf{J}_z$ in the bordered system, or the Floquet approach using $\tilde{\mathbf{B}}$.

During the continuation procedure, the computation of the derivatives of the additional equation is required. As shown by Govaerts[37], in the case of the bordering technique, analytical expressions for the derivatives of g with respect to one of the two active parameters α are found as

$$g_\alpha = -\mathbf{v}^* \mathbf{G}_\alpha \mathbf{w} \tag{36}$$

where $\mathbf{G}_\alpha$ is the derivative of $\mathbf{G}$ with respect to α, and where $\mathbf{w}$ and $\mathbf{v}$ comes from the resolution of the bordered system and its transposed version:

$$\begin{bmatrix} \mathbf{G} & \mathbf{p} \\ \mathbf{q}^* & 0 \end{bmatrix} \begin{bmatrix} \mathbf{w} \\ g \end{bmatrix} = \begin{bmatrix} \mathbf{0} \\ 1 \end{bmatrix} \tag{37}$$

$$\begin{bmatrix} \mathbf{G} & \mathbf{p} \\ \mathbf{q}^* & 0 \end{bmatrix}^* \begin{bmatrix} \mathbf{v} \\ e \end{bmatrix} = \begin{bmatrix} \mathbf{0} \\ 1 \end{bmatrix} \tag{38}$$

As a result, the only term that has to be evaluated is $\mathbf{G}_\alpha$. For g_{BP} and $g_{F,1}$, this gives

$$\frac{\partial}{\partial \alpha} \left(\mathbf{G}_{BP} \right) = \frac{\partial}{\partial \alpha} \left(\mathbf{G}_{F,1} \right) = \mathbf{J}_{z\alpha} \tag{39}$$

where $\mathbf{J}_{z\alpha}$ is the derivative of the jacobian $\mathbf{J}_z$ with respect to α, that can be computed through finite differences.

In the case of the Floquet approach, the derivatives read

$$\begin{array}{rcl} \frac{\partial}{\partial \alpha} \left(\mathbf{G}_{F,2} \right) & = & \frac{\partial}{\partial \alpha} \left(\tilde{\mathbf{B}} \right) \\ \frac{\partial}{\partial \alpha} \left(\mathbf{G}_{NS} \right) & = & \frac{\partial}{\partial \alpha} \left(\tilde{\mathbf{B}}_\odot \right) = \left(\frac{\partial}{\partial \alpha} \left(\tilde{\mathbf{B}} \right) \right)_\odot \end{array} \tag{40}$$

One could directly rely on finite differences to compute the derivatives of the Floquet exponents in $\tilde{\mathbf{B}}$, that are

$$\frac{\partial}{\partial \alpha} \left(\tilde{\mathbf{B}} \right) = \begin{bmatrix} \frac{\partial \tilde{\lambda}_1}{\partial \alpha} & & & \\ & \frac{\partial \tilde{\lambda}_2}{\partial \alpha} & & \\ & & \ddots & \\ & & & \frac{\partial \tilde{\lambda}_{2n}}{\partial \alpha} \end{bmatrix} \tag{41}$$

However, this means that the eigenvalue problem (20) has to be solved $N_H + 2$ times per iteration, which is cumbersome for large systems. Instead, in this paper one computes these expressions using the properties of the derivatives of eigenvalues demonstrated by Van der Aa *et al.*[40]. Denoting $\mathbf{\Lambda}$ the eigenvector matrix of $\mathbf{B}$, and $\boldsymbol{\xi}$ the localization vector containing the index of the $2n$ Floquet exponents $\tilde{\boldsymbol{\lambda}}$ among the eigenvalues $\boldsymbol{\lambda}$, i.e.,

$$\tilde{\lambda}_i = \lambda_{\xi_i} \tag{42}$$

the eigenvalues derivatives can be computed as

$$\frac{\partial \tilde{\lambda}_i}{\partial \alpha} = \left(\mathbf{\Lambda}^{-1} \frac{\partial \mathbf{B}}{\partial \alpha} \mathbf{\Lambda} \right)_{(\xi_i, \xi_i)} \tag{43}$$

The only terms to be computed are thus the derivatives of $\mathbf{B}$, whose expression can be obtained from equations (21-22). This requires the computation of the derivative of the jacobian $\mathbf{J}_z$ with respect to α, which can be performed using finite differences.

3 VALIDATION OF THE METHOD ON THE STUDY OF AN INDUSTRIAL, COMPLEX MODEL WITH STRONG NONLINEARITIES: THE SMALLSAT

In this section, the HB method is used to address the continuation of periodic solutions of a large-scale structure, and the detection and tracking of their bifurcations. Analysis of nonlinear phenomena such as frequency/amplitude jumps and quasiperiodic oscillations is carried out using the outlined method.

3.1 Case study: SmallSat spacecraft

The example studied is referred to as the *SmallSat*, a structure represented in Figure 1(a) and which was conceived by EADS-Astrium as a platform for small satellites. The interface between the spacecraft and launch vehicle is achieved via four aluminum brackets located around cut-outs at the base of the structure. The total mass of the spacecraft including the interface brackets is around $64\,\text{kg}$, it is $1.2\,\text{m}$ in height and $1\,\text{m}$ in width. It supports a dummy telescope mounted on a baseplate through a tripod, and the telescope plate is connected to the SmallSat top floor by three shock attenuators, termed *shock attenuation systems for spacecraft and adaptor* (SASSAs), whose dynamic behavior may exhibit nonlinearity.

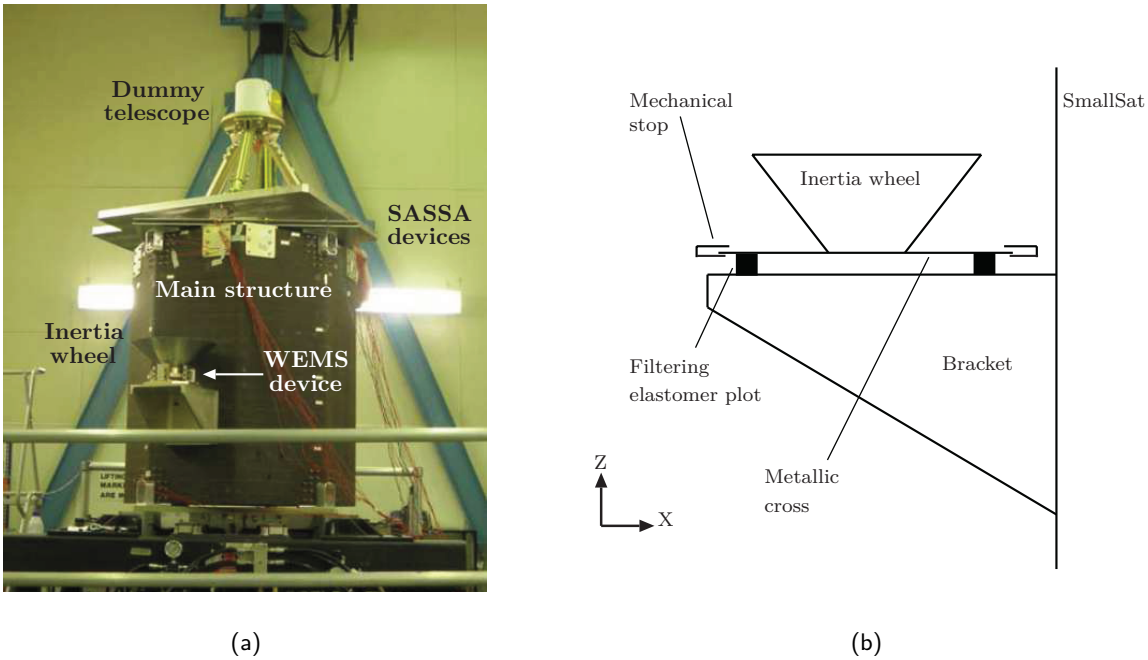

(a) (b)

Figure 1: SmallSat spacecraft equipped with an inertia wheel supported by the WEMS and a dummy telescope connected to the main structure by the SASSA isolators. (a) Photograph. (b) Schematic of the nonlinear vibration isolation device.

Besides, as depicted in Figure 1(b), a support bracket connects to one of the eight walls the so-called *wheel elastomer mounting system* (WEMS) device which is loaded with an 8-kg dummy inertia wheel. The WEMS device is a mechanical filter which mitigates disturbances coming from the inertia wheel through the presence of a soft elastomeric interface between its mobile part, i.e. the inertia wheel and a supporting metallic cross, and its fixed part, i.e. the bracket and by extension the spacecraft. Moreover, eight mechanical stops limit the axial and lateral motions of the WEMS mobile part during launch, which gives rise to strongly nonlinear dynamical phenomena. A thin layer of elastomer placed onto the stops is used to prevent metal-metal impacts. Figure 2(a) presents a simplified though relevant modelling of the WEMS device where the inertia wheel, owing to its important rigidity, is seen as a point mass. The four nonlinear connections (NCs) between the WEMS mobile and fixed parts are labelled NC1 – 4. Each NC possesses a trilinear spring in the axial direction (elastomer in traction/compression plus two stops), a bilinear spring in the radial direction (elastomer in shear plus one stop) and a linear spring in the third direction (elastomer in shear). In Figure 2(a), linear and nonlinear springs are denoted by squares and circles, respectively.

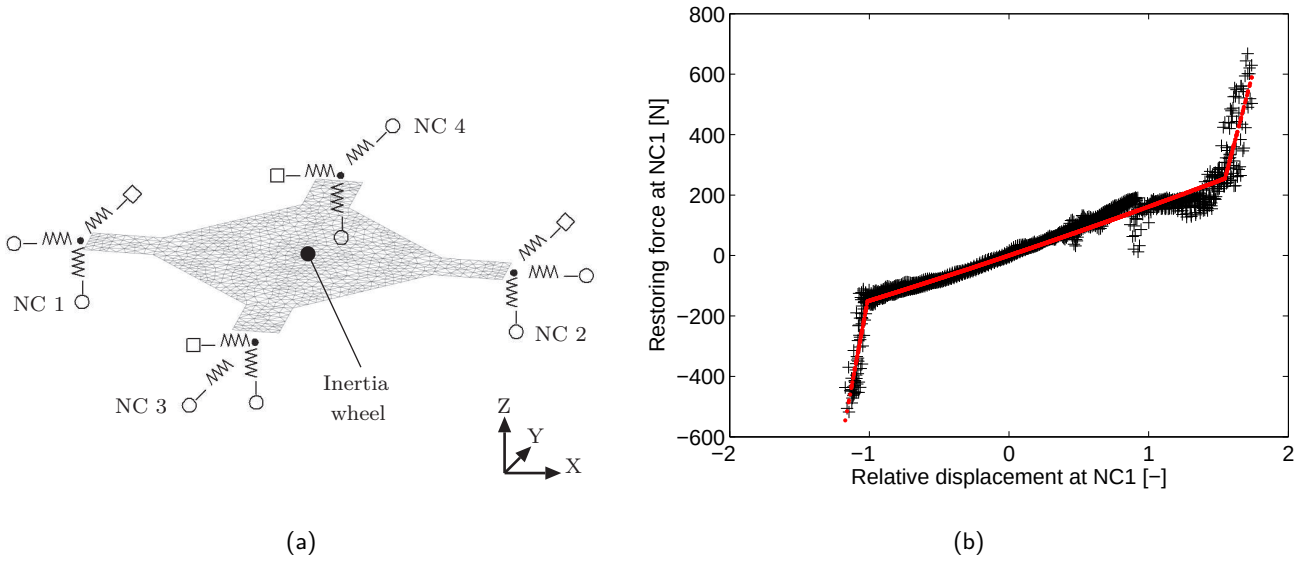

(a) (b)

Figure 2: WEMS. (a) Simplified modeling of the WEMS mobile part considering the inertia wheel as a point mass. The linear and nonlinear connections between the WEMS mobile and fixed parts are signaled by squares and circles, respectively. (b) Experimental stiffness curve of NC1 constructed using the restoring force surface method (in black) and fitted with a trilinear model (in red).

A finite element model (FEM) of the SmallSat was developed and used in the present work to conduct numerical experiments. It comprises about 150,000 DOFs and the comparison with experimental data revealed its good predictive capabilities. The model consists of shell elements (octagon structure and top floor, instrument baseplate, bracket and WEMS metallic cross) and point masses (dummy inertia wheel and telescope) and meets boundary conditions with four clamped nodes. Proportional damping is considered and the high dissipation in the elastomer components of the WEMS is described using lumped dashpots with coefficients $c_{ax} = 63\,\text{Ns/m}$ and $c_{lat} = 37\,\text{Ns/m}$ for axial (vertical) and lateral directions, respectively; this results in a highly non-proportional damping matrix. Then, to achieve tractable nonlinear calculations, the linear elements of the FEM were condensed using the Craig-Bampton reduction technique. This approach consists in expressing the system dynamics in terms of some retained DOFs and internal modes of vibration. Specifically, the full-scale model of the spacecraft was reduced to 9 nodes (excluding DOFs in rotation), namely both sides of each NC and the vertical DOF of the inertia wheel, with 10 internal modes. In total, the reduced-order model thus contains 37 DOFs. Bilinear and trilinear springs were finally introduced within the WEMS module between the NC nodes to model the nonlinearities of the connections between the WEMS and the rest of the SmallSat. To avoid numerical issues, regularization with third-order polynomials was utilized in the close vicinity of the clearances to implement C^1 continuity. The WEMS nonlinearities are the only nonlinear components introduced in the model. They were accurately identified in [2] using measured data from swept-sine base excitations at different amplitude levels. For instance, the stiffness curve characterizing NC1, identified using the restoring force surface method[41], is depicted in Figure 2(b). For confidentiality, clearances and displacements of the SmallSat are given through adimensionalised quantities throughout the paper.

3.2 Nonlinear dynamics and bifurcations of the SmallSat

The first part of the study of the SmallSat is carried out on the forced response of the structure for vertical excitations on the DOF of the inertia wheel. The frequency range of interest is located around the 6th mode of the structure, which corresponds to a linear frequency of 28.75 Hz. However, it was shown by Renson *et al.*[3] that this nonlinear mode undergoes a substantial increase in frequency due to the frequency-energy dependence of the structure.

Figure 3(a) gives the response of the NC1-Z node to a swept-sine excitation of forcing amplitude $F = 155$ N applied vertically on the inertia wheel. For this result and other swept-sine excitations throughout this paper, the applied sweep rate is 10 Hz/min. One first notices a sudden amplitude jump close to 35 Hz, which is expected for a hardening structure. Another zone of high amplitude also appears between 30 and 32 Hz, which is more surprising. A time response of the system to a single harmonic excitation of forcing amplitude $F = 155$ N and frequency $\omega = 30.5$ Hz is provided in Figure 3(b), i.e. in the frequency interval of the unexpected resonance. One observes that quasiperiodic oscillations occur for this operation regime, which is another phenomenon peculiar to nonlinear systems. In this case however, their importance has to be carefully assessed since they have amplitude as large as the one of the resonance.

Increasing the forcing amplitude of the swept-sine excitation further, one obtains the 4 responses given in Figure 3(c) corresponding to small variations of F between 168 and 174 N. Although the responses do not significantly evolve from 168 to 170 N and from 172 to 174 N, a substantial increase in frequency and amplitude can be observed when the forcing amplitude varies from 170 to 172 N. This phenomenon, which is not often described in the technical literature, is of high interest since it leads to a resonance frequency shift of almost 4 Hz for a forcing amplitude barely increased by 2 N. For space applications with drastic structural requirements, such a behavior certainly has to be analyzed. Moreover, one notices that the quasiperiodic region is also present for these high excitation levels.

In order to explain and study the nonlinear phenomena highlighted, the HB method presented in this paper is now applied to the model. Figure 4(a) depicts the system's frequency response curve computed with $N_H = 9$ harmonics retained in the Fourier approximation and $N = 1024$ points per period. For this result and others in the paper, no subharmonic solution is sought ($\nu = 1$). The amplitude of the periodic solutions computed is represented, that is the maximum displacement of the DOF of interest along the period. The evolution of the harmonic coefficients $\boldsymbol{\sigma}_i$ $(i = 1, \ldots, N_H)$ along the branch is given in Figure 4(b), where the following normalization is applied:

$$\begin{aligned} \boldsymbol{\sigma}_0 &= c_0^x \\ \boldsymbol{\sigma}_i &= \frac{\sqrt{\left(\mathtt{s}_i^x\right)^2+\left(\mathtt{c}_i^x\right)^2}}{\sum_{k=1}^{N_H}\sqrt{\left(\mathtt{s}_k^x\right)^2+\left(\mathtt{c}_k^x\right)^2}} \quad (i = 1, \ldots, N_H) \end{aligned} \tag{44}$$

From 20 to 23 Hz, only the fundamental frequency is present in the response. When the excitation enters the resonance region, the nonlinearities of the SmallSat activate other harmonics in the response such as the second and third ones. From the figure, it is also clear that the 6th and higher harmonics have a negligible participation to the response; for this reason, a number of harmonics $N_H = 5$ retained in the Fourier series is considered throughout the rest of the paper. It is also possible to show that the number of $N = 1024$ points per period is sufficient to capture the dynamics in play.

Circle and triangle markers denote the fold and NS bifurcations, respectively, that are detected along the branch in Figure 4(a). One observes that a pair of fold bifurcations is present in the bending segments of the resonance peak, which is due to the hardening behavior of the system. Indeed, fold bifurcations give rise to a change in stability of the periodic solutions, which explains the jump phenomenon from high to low amplitude in Figures 3(a) and (c). One also notices a pair of NS bifurcations, which means that quasiperiodic solutions can be found in their vicinity. As a verification, frequency responses computed with HB method are superimposed to swept-sine responses in Figures 5(a) and (b), for forcing amplitude $F = 155$ N and 174 N, respectively. Along with the fact that the frequency responses provide accurate estimations of the displacement envelopes, as expected, one also notes that the bifurcations are directly related to the nonlinear phenomena observed. On the one hand, fold bifurcations accurately point out the location of the amplitude jump; tracking the evolution of fold bifurcations with respect to other parameters such as the forcing amplitude F or the axial damping c_{ax} could then reveal the mechanism of the phenomenon shown in Figure 3(c). On the other hand, the large quasiperiodic oscillations observed in Figures 3(a) and (b) are created and eliminated at the first and second NS bifurcations, respectively; tracking the evolution of NS bifurcations with respect to a design parameter such as the axial damping c_{ax} could then indicate how one can modify the design of the SmallSat to avoid such disturbances.

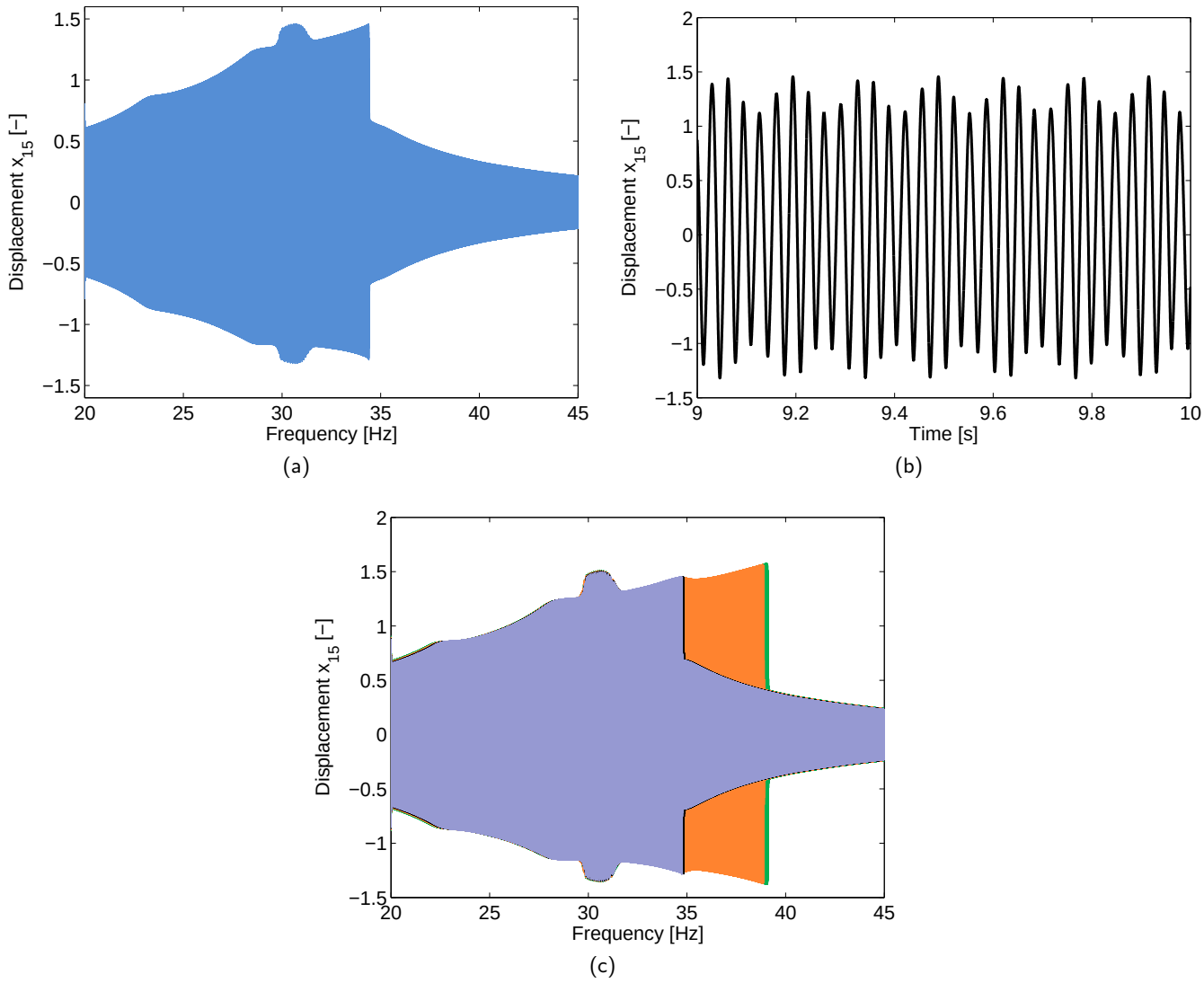

Figure 3: Nonlinear dynamics of the SmallSat. Time responses of the NC1-Z node of the SmallSat for different excitations applied to the inertia wheel. (a) Swept-sine excitation of amplitude $F = 155$ N. (b) Harmonic excitation of amplitude $F = 155$ N and frequency $\omega = 30.5$ Hz. (c) Swept-sine excitations of amplitudes $F = 168$ N (purple curve), 170 N (black curve), 172 N (orange curve) and 174 N (green curve).

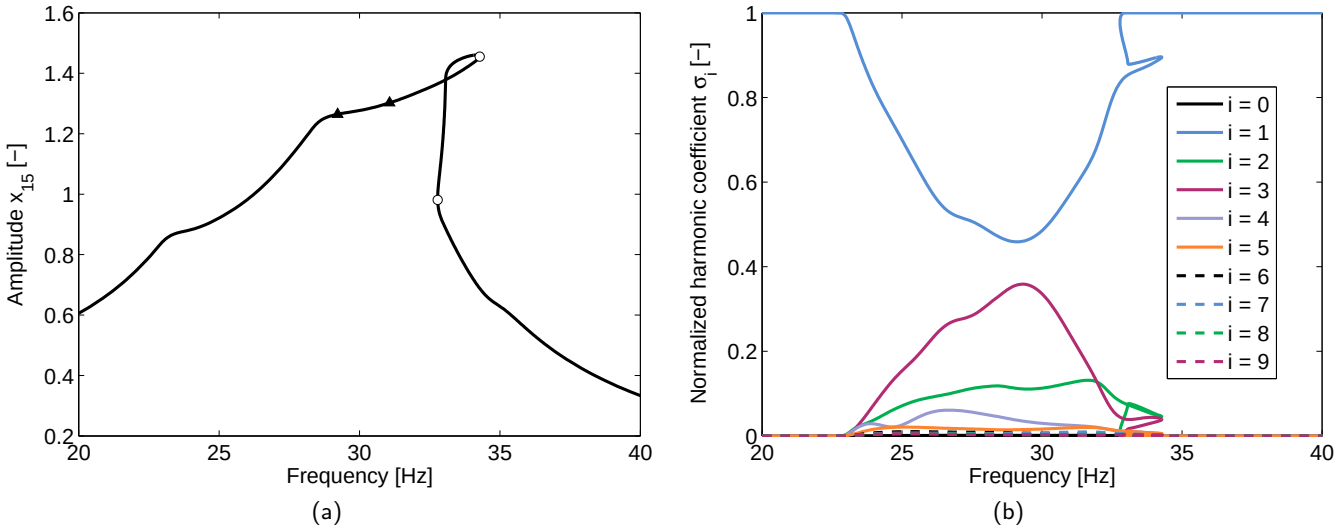

Figure 4: SmallSat frequency response at NC1-Z node for harmonic excitations of amplitude $F = 155\,\mathrm{N}$ applied to the inertia wheel, obtained with the HB method. (a) Displacement responses with markers ○ and ▲ depicting fold and NS bifurcations, respectively. (b) Harmonic coefficients responses.

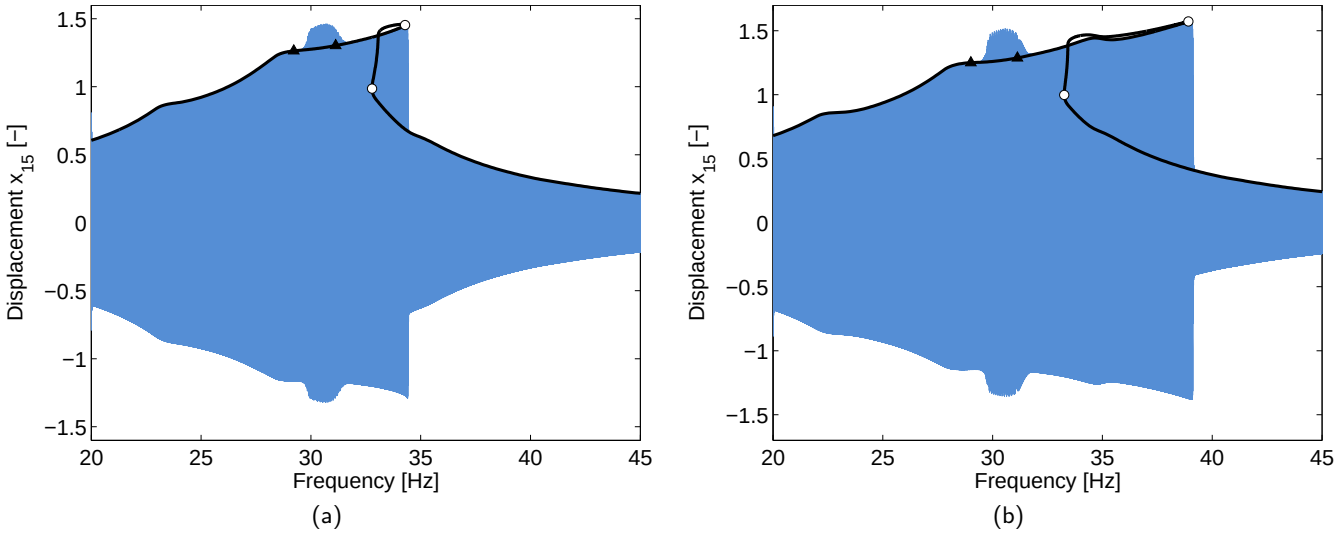

Figure 5: SmallSat displacement response at NC1-Z node for excitations of amplitude (a) $F = 155\,\mathrm{N}$ and (b) $F = 174\,\mathrm{N}$ applied to the inertia wheel. The blue lines represent the swept-sine response obtained from time simulation, and the black lines are the frequency responses obtained with the HB method. Markers ○ and ▲ depict fold and NS bifurcations, respectively.

3.3 Influence of the forcing amplitude F and the axial damping c_{ax} on the fold bifurcations

The purpose of this section is to get a deeper understanding of the frequency/jump phenomenon occurring close to the fold bifurcations. To this end, a tracking of the fold bifurcations in the codimension-2 forcing frequency-ω and amplitude-F space is performed using the technique developed in section 2.5. Figure 6(a) represents the fold curve obtained, together with the frequency responses of the system for different forcing levels. Figure 6(b) also shows the projection of this curve in the F-amplitude plane. Very interestingly, the fold branch first tracks the bifurcations of the main frequency response, and then turns back to reveal *detached resonance curves* (DRC), or *isolas*, that are rarely observed for such large systems. These DRCs are created around the resonance peak at a forcing amplitude $F = 158\,\text{N}$, then expands both in frequency and amplitude, until one reaches a forcing amplitude $F = 170\,\text{N}$ at which they merge with this resonance peak. It can be shown that the upper part of the DRCs is stable; as a direct consequence, the merging of the DRC with the resonance peak leads to the sudden increase of the latter in frequency and amplitude, as highlighted in Figure 3(c).

Another fold curve is computed for a configuration of the SmallSat with $c_{ax} = 85\,\text{Ns/m}$, and represented in dashed line in Figure 6(b). While we could expect from an increase in the damping to annihilate nonlinear phenomena such as DRC, one sees that it only postpones the merging to higher forcing amplitudes and does not alter the size of the DRCs. For this system, DRCs are thus robust and deserve a careful investigation from the structural engineers.

Together with the explanations about the SmallSat dynamics they provide, these first results show that crucial information can be missed when one only performs continuation of periodic solutions. Obviously, a tracking in codimension-2 space is necessary in order to reveal DRCs.

3.4 Influence of the axial damping c_{ax} on the NS bifurcations

Focusing now on NS bifurcations, one can also apply the continuation procedure presented in section 2.5 to study the effect of a design parameter of the system such as c_{ax} on the quasiperiodic oscillations. Figure 7(a) depicts the evolution of the NS curve in the codimension-2 forcing frequency-ω and axial damping c_{ax} space, to which one superimposes frequency responses computed for $c_{ax} = 63\,\text{Ns/m}$, $80\,\text{Ns/m}$ and $85\,\text{Ns/m}$. Its projection in the c_{ax}-amplitude plane is also given in Figure 7(b). It is interesting to note that increasing the axial damping up to a value of $84\,\text{Ns/m}$ eliminates the NS bifurcations, while it does not significantly affect the resonance peaks.

As a verification, Figure 8 shows the influence of c_{ax} on a displacement response for swept-sine excitations. At a forcing amplitude $F = 155\,\text{N}$ and for an axial damping $c_{ax} = 63\,\text{Ns/m}$, the quasiperiodic oscillations represent the part of the response with the largest amplitude. Increasing c_{ax} up to $85\,\text{Ns/m}$ eliminates the NS bifurcations which generate these disturbances, with a small impact on the frequency of the resonance.

4 CONCLUSIONS

The purpose of this paper was twofold. First, it intended to extend the harmonic balance method from the computation of periodic solutions to the tracking of their bifurcations in codimension-2 parameter space. To this end, continuation techniques were adapted in order to obtain a robust and efficient algorithm able to deal with large engineering structures.

In the second part of this paper the HB method and its extension were applied to the SmallSat spacecraft, an industrial and complex model with several localized nonlinearities. Performing swept-sine excitation study on this structure revealed two types of nonlinear phenomena, namely quasiperiodic oscillations and frequency/amplitude jump due to detached resonance curves, which also involved responses of high amplitude. One then illustrated how the detection and tracking of fold and NS bifurcations can explain these phenomena, and how the design parameters of the system can be tuned to reduce their effects.

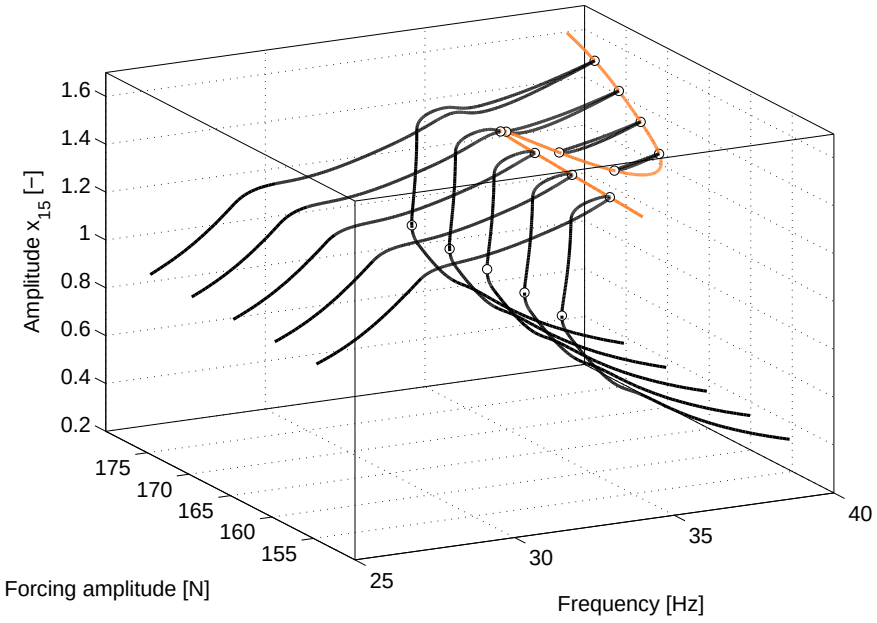

(a)

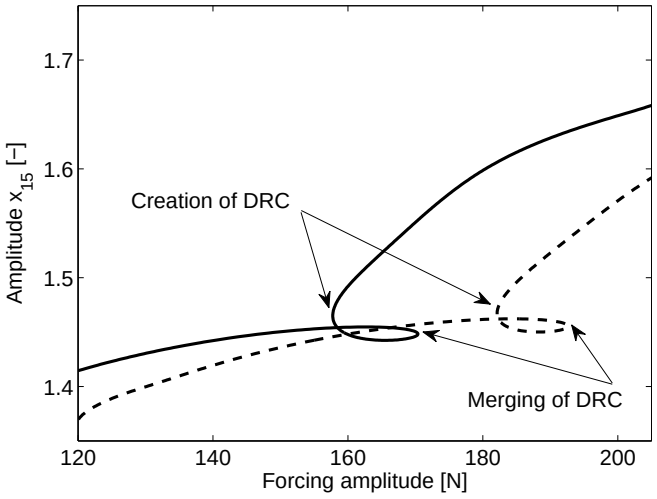

(b)

Figure 6: Merging of the detached resonance curve with the main frequency response. (a) The orange line represents the branch of fold bifurcations tracked with respect to the excitation amplitude F and frequency ω. Frequency responses of the NC1-Z node for harmonic excitations of amplitude $F = 155\,\text{N}$, $160\,\text{N}$, $170\,\text{N}$ and $175\,\text{N}$ are also given with the black lines. Markers $\circ$ depict fold bifurcations. (b) Projection of the branch of fold bifurcations on the F-amplitude plane. The solid and dashed lines represent the branches for $c_{ax} = 63\,\text{Ns/m}$ (reference) and $85\,\text{Ns/m}$, respectively.

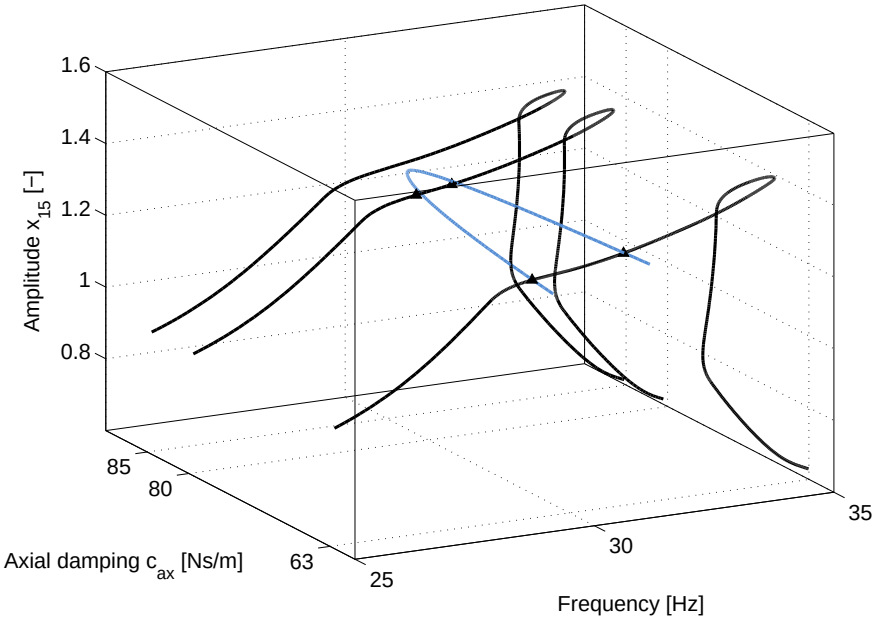

(a)

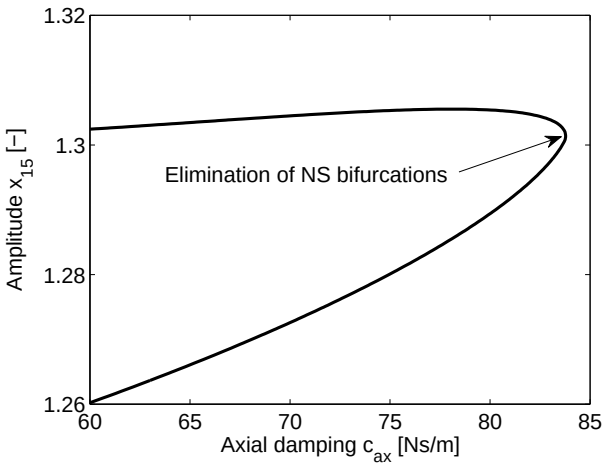

(b)

Figure 7: Elimination of the NS bifurcations. (a) The blue line represents the branch of NS bifurcations tracked with respect to the axial damping coefficient c_{ax} and frequency ω. Frequency responses of the NC1-Z node for harmonic excitations of amplitude $F = 155$ N, and for configurations with $c_{ax} = 63$ Ns/m (reference), 80 Ns/m and 85 Ns/m are also given with the black lines. Markers ▲ depict NS bifurcations. (b) Projection of the branch of NS bifurcations on the c_{ax}-amplitude plane.

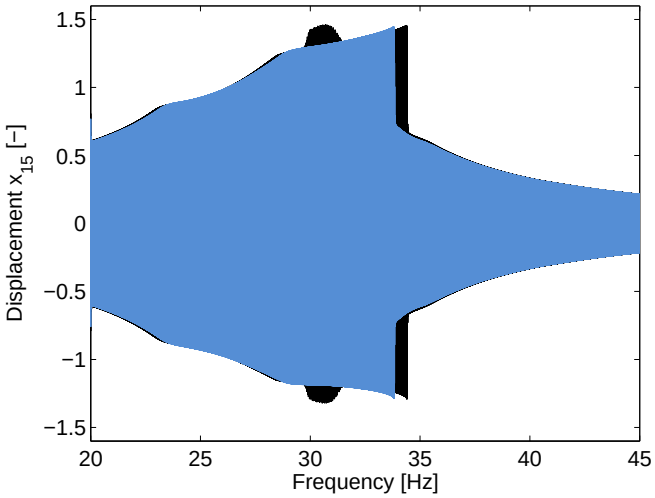

Figure 8: SmallSat displacement response at NC1-Z node for swept-sine excitations of amplitude $F = 155$ N applied to the inertia wheel. The blue line and green line represent configuration with $c_{ax} = 63$ Ns/m (reference) and 85 Ns/m, respectively.

ACKNOWLEDGMENTS

The authors Thibaut Detroux, Luc Masset and Gaetan Kerschen would like to acknowledge the financial support of the European Union (ERC Starting Grant NoVib 307265).

References

[1] **Nayfeh, A. H.** and **Mook, D. T.**, Nonlinear oscillations, John Wiley & Sons, 2008.

[2] **Noël, J., Renson, L.** and **Kerschen, G.**, *Complex dynamics of a nonlinear aerospace structure: Experimental identification and modal interactions*, Journal of Sound and Vibration, Vol. 333, No. 12, pp. 2588–2607, 2014.

[3] **Renson, L., Noël, J.** and **Kerschen, G.**, *Complex dynamics of a nonlinear aerospace structure: numerical continuation and normal modes*, Nonlinear Dynamics, pp. 1–17, 2014.

[4] **Denegri, C. M.**, *Limit cycle oscillation flight test results of a fighter with external stores*, Journal of Aircraft, Vol. 37, No. 5, pp. 761–769, 2000.

[5] **Ahlquist, J. R., Carreño, J. M., Climent, H., de Diego, R.** and **de Alba, J.**, *Assessment of nonlinear structural response in A400M GVT*, *Structural Dynamics, Volume 3*, pp. 1147–1155, Springer, 2011.

[6] **Noël, J.-P., Renson, L., Kerschen, G., Peeters, B., Manzato, S.** and **Debille, J.**, *Nonlinear dynamic analysis of an F-16 aircraft using GVT data*, *Proceedings of the International Forum on Aeroelasticity and Structural Dynamics*, 2013.

[7] **Padmanabhan, C.** and **Singh, R.**, *Analysis of periodically excited non-linear systems by a parametric continuation technique*, Journal of Sound and Vibration, Vol. 184, No. 1, pp. 35–58, 1995.

[8] **Peeters, M., Viguié, R., Sérandour, G., Kerschen, G.** and **Golinval, J.-C.**, *Nonlinear normal modes, Part II: Toward a practical computation using numerical continuation techniques*, Mechanical systems and signal processing, Vol. 23, No. 1, pp. 195–216, 2009.

[9] **Doedel, E. J., Champneys, A. R., Fairgrieve, T. F., Kuznetsov, Y. A., Sandstede, B.** and **Wang, X.**, AUTO97*: Continuation and bifurcation software for ordinary differential equations (with HomCont)*, User's Guide, Concordia University, Montreal, Canada, Available from http://indy.cs.concordia.ca, 1997.

[10] **Ascher, U., Christiansen, J.** and **Russell, R. D.**, *A collocation solver for mixed order systems of boundary value problems*, Mathematics of Computation, pp. 659–679, 1979.

[11] **Kuznetsov, Y. A.** and **Levitin, V. V.**, CONTENT*: A multiplatform environment for analyzing dynamical systems*, User's Guide, Dynamical Systems Laboratory, CWI, Amsterdam, Netherlands, Available by anonymous ftp from ftp.cwi.nl/pub/CONTENT, 1995-1997.

[12] **Dhooge, A., Govaerts, W.** and **Kuznetsov, Y. A.**, *MATCONT: a MATLAB package for numerical bifurcation analysis of ODEs*, ACM Transactions on Mathematical Software (TOMS), Vol. 29, No. 2, pp. 141–164, 2003.

[13] **Dankowicz, H.** and **Schilder, F.**, *An Extended Continuation Problem for Bifurcation Analysis in the Presence of Constraints*, Journal of Computational and Nonlinear Dynamics, Vol. 6, No. 3, 2011.

[14] **Kundert, K. S.** and **Sangiovanni-Vincentelli, A.**, *Simulation of nonlinear circuits in the frequency domain*, IEEE Transactions on Computer-Aided Design of Integrated Circuits and Systems, Vol. 5, No. 4, pp. 521–535, 1986.

[15] **Cardona, A., Coune, T., Lerusse, A.** and **Geradin, M.**, *A multiharmonic method for non-linear vibration analysis*, International Journal for Numerical Methods in Engineering, Vol. 37, No. 9, pp. 1593–1608, 1994.

[16] **von Groll, G.** and **Ewins, D. J.**, *The harmonic balance method with arc-length continuation in rotor/stator contact problems*, Journal of Sound and Vibration, Vol. 241, No. 2, pp. 223–233, 2001.

[17] **Laxalde, D.** and **Thouverez, F.**, *Complex non-linear modal analysis for mechanical systems: Application to turbomachinery bladings with friction interfaces*, Journal of sound and vibration, Vol. 322, No. 4, pp. 1009–1025, 2009.

[18] **Grolet, A.** and **Thouverez, F.**, *On a new harmonic selection technique for harmonic balance method*, Mechanical Systems and Signal Processing, Vol. 30, pp. 43–60, 2012.

[19] **Grolet, A.** and **Thouverez, F.**, *Vibration of mechanical systems with geometric nonlinearities: Solving Harmonic Balance Equations with Groebner basis and continuations methods*, *Proceedings of the Colloquium Calcul des Structures et Modélisation CSMA*, Giens, France, 2013.

[20] **Arquier, R.**, Une méthode de calcul des modes de vibrations non-linéaires de structures, Ph.D. thesis, Université de la méditerranée (Aix-Marseille II), Marseille, France, 2007.

[21] **Cochelin, B.** and **Vergez, C.**, *A high order purely frequency-based harmonic balance formulation for continuation of periodic solutions*, Journal of sound and vibration, Vol. 324, No. 1, pp. 243–262, 2009.

[22] **Karkar, S., Cochelin, B.** and **Vergez, C.**, *A comparative study of the harmonic balance method and the orthogonal collocation method on stiff nonlinear systems*, Journal of Sound and Vibration, Vol. 333, No. 12, pp. 2554–2567, 2014.

[23] **Detroux, T., Renson, L.** and **Kerschen, G.**, *The harmonic balance method for advanced analysis and design of nonlinear mechanical systems*, *Nonlinear Dynamics, Volume 2*, pp. 19–34, Springer, 2014.

[24] **Petrov, E.** and **Ewins, D.**, *Analytical formulation of friction interface elements for analysis of nonlinear multi-harmonic vibrations of bladed disks*, Journal of turbomachinery, Vol. 125, No. 2, pp. 364–371, 2003.

[25] **Lau, S.** and **Zhang, W.-S.**, *Nonlinear vibrations of piecewise-linear systems by incremental harmonic balance method*, Journal of Applied Mechanics, Vol. 59, pp. 153, 1992.

[26] **Pierre, C., Ferri, A.** and **Dowell, E.**, *Multi-harmonic analysis of dry friction damped systems using an incremental harmonic balance method*, Journal of applied mechanics, Vol. 52, No. 4, pp. 958–964, 1985.

[27] **Cameron, T.** and **Griffin, J.**, *An alternating frequency/time domain method for calculating the steady-state response of nonlinear dynamic systems*, Journal of Applied Mechanics, Vol. 56, No. 1, pp. 149–154, 1989.

[28] **Narayanan, S.** and **Sekar, P.**, *A frequency domain based numeric–analytical method for non-linear dynamical systems*, Journal of sound and vibration, Vol. 211, No. 3, pp. 409–424, 1998.

[29] **Bonani, F.** and **Gilli, M.**, *Analysis of stability and bifurcations of limit cycles in Chua's circuit through the harmonic-balance approach*, Circuits and Systems I: Fundamental Theory and Applications, IEEE Transactions on, Vol. 46, No. 8, pp. 881–890, 1999.

[30] **Duan, C.** and **Singh, R.**, *Super-harmonics in a torsional system with dry friction path subject to harmonic excitation under a mean torque*, Journal of Sound and Vibration, Vol. 285, No. 4, pp. 803–834, 2005.

[31] **Kim, T., Rook, T.** and **Singh, R.**, *Super-and sub-harmonic response calculations for a torsional system with clearance nonlinearity using the harmonic balance method*, Journal of Sound and Vibration, Vol. 281, No. 3, pp. 965–993, 2005.

[32] **Lazarus, A.** and **Thomas, O.**, *A harmonic-based method for computing the stability of periodic solutions of dynamical systems*, Comptes Rendus Mécanique, Vol. 338, No. 9, pp. 510–517, 2010.

[33] **Moore, G.**, *Floquet theory as a computational tool*, SIAM journal on numerical analysis, Vol. 42, No. 6, pp. 2522–2568, 2005.

[34] **Seydel, R.**, Practical bifurcation and stability analysis, Springer, 2010.

[35] **Govaerts, W., Kuznetsov, Y. A., De Witte, V., Dhooge, A., Meijer, H., Mestrom, W., Riet, A.** and **Sautois, B.**, *MATCONT and CL MATCONT: Continuation toolboxes in matlab*, Gent University and Utrech University, Tech. Rep, 2011.

[36] **Guckenheimer, J., Myers, M.** and **Sturmfels, B.**, *Computing hopf bifurcations I*, SIAM Journal on Numerical Analysis, Vol. 34, No. 1, pp. 1–21, 1997.

[37] **Govaerts, W. J.**, Numerical methods for bifurcations of dynamical equilibria, Vol. 66, Siam, 2000.

[38] **Beyn, W.-J., Champneys, A., Doedel, E., Govaerts, W., Kuznetsov, Y. A.** and **Sandstede, B.**, *Numerical continuation, and computation of normal forms*, Handbook of dynamical systems, Vol. 2, pp. 149–219, 2002.

[39] **Doedel, E. J., Govaerts, W.** and **Kuznetsov, Y. A.**, *Computation of periodic solution bifurcations in ODEs using bordered systems*, SIAM Journal on Numerical Analysis, Vol. 41, No. 2, pp. 401–435, 2003.

[40] **Van Der Aa, N., Ter Morsche, H.** and **Mattheij, R.**, *Computation of eigenvalue and eigenvector derivatives for a general complex-valued eigensystem*, Electronic Journal of Linear Algebra, Vol. 16, No. 1, pp. 300–314, 2007.

[41] **Masri, S.** and **Caughey, T.**, *A nonparametric identification technique for nonlinear dynamic problems*, Journal of Applied Mechanics, Vol. 46, No. 2, pp. 433–447, 1979.